Deformation of Aluminium Sheet at Elevated Temperatures

Experiments and Modelling

L. van Haaren

November 2002

Master's Thesis
Section Mechanics of Forming Processes
Department of Mechanical Engineering
University of Twente
Enschede, The Netherlands

Abstract

There is a growing demand to reduce the weight of vehicles in order to minimise energy consumption and air pollution. To accomplish this weight reduction, car body panels could be made of aluminium sheet, which has a better strength to weight ratio than traditionally used mild steel. The formability of aluminium is less than that of mild steel, but it can be improved by deforming aluminium at elevated temperatures.

Since there is not much experience in industry in deforming aluminium sheet at elevated temperatures and trial and error in the workshop is very expensive, numerical simulations are used to predict and optimise the deformation process. To accurately simulate a deformation process it is necessary to know and model the material behaviour.

The purpose of this graduation project is to develop a material model for aluminium that takes variations in temperature and strain rate into account. Two different material models have been examined: a phenomenological model (extended Nadai model) and a physically based model (Bergström model). The parameters of these models have been determined using the results of experiments performed at TNO Eindhoven. These experiments have been conducted for various constant strain rates and temperatures. It was seen that both material models describe the constant strain rate experiments reasonably well and that the Bergström model performs slightly better than the extended Nadai model. A number of numerical simulations have been performed to demonstrate the applicability of the Bergström model.

When a strain rate jump is applied, large differences between the models appear. The extended Nadai model describes an instantaneous response and the Bergström model describes a more gradual response. To determine which of the models predicts the behaviour best, tensile tests with a strain rate jump have been performed at the University of Twente. It was concluded that the actual material behaviour in case of a strain rate jump is somewhere in the middle of the two material models.

Samenvatting

Er is een groeiende vraag naar voertuigen met een lager gewicht om het energieverbruik en de uitstoot van schadelijke stoffen te verminderen. Deze gewichtsvermindering kan worden gerealiseerd door het plaatwerk van aluminium te maken. Aluminium heeft namelijk een betere sterkte-gewichtsverhouding dan staal. De vervormbaarheid van aluminium is echter slechter dan die van het gebruikelijke dieptrekstaal. Deze vervormbaarheid kan worden verbeterd door aluminium bij hogere temperaturen te verwerken.

Omdat er weinig ervaring is met het omvormen van aluminium bij hogere temperaturen en het duur is om dit simpelweg uit te proberen, is het belangrijk om numerieke simulaties te gebruiken om dit proces te kunnen voorspellen en optimaliseren. Om dit correct te kunnen doen is het nodig om het materiaalgedrag van aluminium bij hogere temperaturen te kennen en te beschrijven met behulp van een model.

Het doel van dit afstudeerproject is het ontwikkelen van een materiaalmodel voor aluminium dat rekening houdt met variaties in de temperatuur en reksnelheid. Twee verschillende materiaalmodellen zijn onderzocht: het fenomenologische extended Nadai model en het op de fysica gebaseerde Bergström model. De parameters van deze modellen zijn bepaald met behulp van experimenten, uitgevoerd bij TNO Eindhoven. Deze experimenten zijn uitgevoerd bij diverse constante reksnelheden en temperaturen. Beide modellen voorspellen het materiaalgedrag redelijk goed. Het Bergström model is beter dan het extended Nadai model. Een aantal numerieke simulaties is uitgevoerd om de toepasbaarheid van het Bergström model te testen.

Als er een sprong in de reksnelheid wordt toegepast treden er grote verschillen tussen de modellen op. Het extended Nadai model geeft een instantane reactie terwijl het Bergström model een meer geleidelijke reactie geeft. Uit experimenten met een reksnelheidssprong uitgevoerd op de Universiteit Twente blijkt dat het eigenlijke materiaalgedrag tussen deze modellen in zit.

Contents

Nomenclature

Symbol	Description
a_1	Material constant for the extended Nadai model
a_2	Material constant for the extended Nadai model
A	Current cross-sectional area
A_0	Initial cross-sectional area
b	Burgers vector
b_1	Material constant for the extended Nadai model
b_2	Material constant for the extended Nadai model
c	Material constant for the extended Nadai model
C	Material constant
C_0	Material constant for the extended Nadai model
C_i	Material constant
C_T	Fitting parameter for the Bergström model
e	Engineering strain
E	Young's modulus of elasticity
F	Tensile force
G	Elastic shear modulus
G_{ref}	Reference value for the shear modulus
k	Boltzmann's constant
L	Current length
L_0	Initial length
m	Strain rate sensitivity
m_0	Material constant for the extended Nadai model
n	Strain hardening coefficient
n_0	Material constant for the extended Nadai model
Q_v	Activation energy
R	Gas constant
S	Engineering stress
T	Temperature
T_1	Fitting parameter for the Bergström model
T^a	Absolute temperature
T_m^a	Absolute melting temperature
T_h	Homologous temperature
T_m	Reference temperature
U	Immobilisation rate of dislocations
U_0	Intrinsic immobilisation rate

Symbol	**Description**
α	Scaling parameter for the Bergström model
ΔG_0	Activation energy
ε	True strain
ε_0	Initial strain
$\dot{\varepsilon}$	Strain rate
$\dot{\varepsilon}_0$	Reference strain rate
ρ	Dislocation density
σ	True stress
σ^*	Dynamic stress
σ_0^*	Maximum value for the dynamic stress
σ_0	Strain rate independent stress
σ_f	Flow stress
σ_w	Contribution of the strain hardening
σ_y	Yield strength
Ω	Remobilisation rate of dislocations
Ω_0	Low temperature, high strain rate limit value of the remobilisation probability

Glossary

Annealing A heat treatment in which a material is exposed to an elevated temperature and then slowly cooled, this is carried out to relieve stresses, increase softness, ductility and toughness or produce a specific microstructure.

Dynamic strain-ageing A material process that causes stretcher lines in aluminium-magnesium alloys that are deformed at room temperature, attributed to the interaction between solute atoms and dislocations.

Engineering strain The change in gauge length of a specimen (in the direction of the applied stress) divided by the original gauge length.

Engineering stress The instantaneous load applied to a specimen divided by the initial cross-sectional area.

Formability The maximum amount of deformation a metal can withstand in a particular process without failing.

Recovery The relief of some of the internal strain energy of a previously cold-worked metal, usually by heat treatment.

Homologous temperature The ratio of the absolute temperature of a material to its absolute melting temperature.

Recrystallisation The formation of a new set of strain-free grains within a previously cold-worked material.

Solid solution A homogeneous crystalline phase that contains two or more chemical species.

Strain hardening The increase in hardness and strength of a ductile metal as it is plastically deformed below its recrystallisation temperature.

Stretcher lines Long vein-like marks appearing on the surface of certain metals, in the direction of the maximum shear stress. Occurs when the metal is subjected to deformation beyond the yield point.

True strain The natural logarithm of the ratio of instantaneous gauge length to the original gauge length of a specimen being deformed by a uniaxial force.

True stress The instantaneous applied load divided by the instantaneous cross-sectional area of a specimen.

Chapter 1

Introduction

In this chapter general background information for this thesis is presented. First the relevance of the research presented in this thesis is described. Subsequently some information about aluminium alloys, metal forming and numerical simulations is given. Finally the outline of this thesis is presented.

1.1 Environmental concerns

In the early seventies the Club of Rome reported a relation between economic growth and contamination of the environment. During the last three decades this environmental pollution has attracted the attention of both politics and public, resulting in a number of laws and measures to protect the environment.

A large contributor to environmental pollution is the transportation sector, which is accountable for about 20 % of the total CO_2 emissions in the Netherlands in the year 2000 (see Figure 1.1). In order to reduce this polluting effect of transport, government

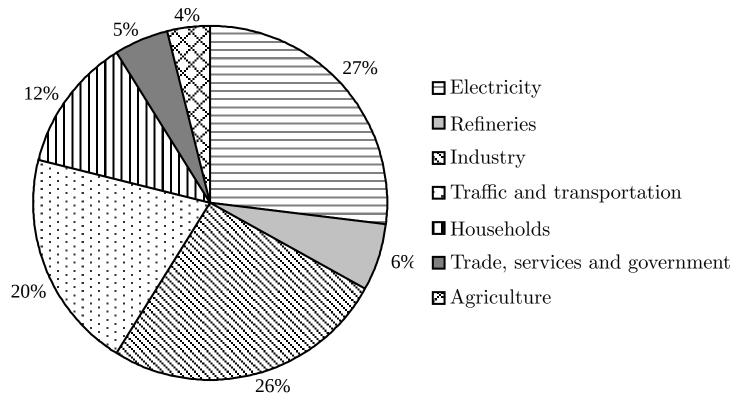

Figure 1.1: CO_2 emissions per sector in the Netherlands in the year 2000 [15]

regulations mandate the automotive industry to reduce vehicle exhaust emissions and to enhance fuel economy.

To meet these imperatives, it is necessary to increase the fuel-efficiency of vehicles by improving engine efficiency, the application of alternative (electrical and hybrid) fuel systems and/or reducing the weight of the vehicle. It is estimated that for every 10 % reduction in vehicle weight, a 5.5 % decrease in fuel consumption can be achieved [13].

As in most automotive applications a reduction in vehicle size is not desired, the required weight reduction should be achieved by replacing 'conventional' mild steel by high-strength low-weight materials. Aluminium is an interesting alternative for mild steel as it has a good strength to weight ratio, a good corrosion resistance and is not too expensive. An example for the applicability of aluminium is the Audi A2 which has an aluminium body: it weighs only 870 kg, an estimated 135 kg less than its (imaginary) steel equivalent.

1.2 Aluminium alloys

Pure aluminium is too soft to be of structural value, hence the aluminium used in industry contains alloying elements. These alloying elements increase the strength without significantly increasing the weight. Next to that, improved machinability, weldability, surface appearance and corrosion resistance can be obtained by adding appropriate elements. The major alloying additions for aluminium are copper, silicon, magnesium, manganese and zinc. The composition is designated by a four-digit number that indicates the principal impurities, see Table 1.1 [6, 7].

Under normal processing conditions, the formability of aluminium sheet is lower than that of deep drawing steel. This means that aluminium can withstand less deformation than deep drawing steel before failure occurs in the production process.

Of all aluminium alloys, aluminium-magnesium alloys (AA 5xxx alloys) have the highest formability. However, this series suffers from stretcher lines, resulting in a poor surface quality. Therefore the AA 5xxx alloys are mostly used for the inner panels

Table 1.1: Aluminium alloys and their principal impurities

Alloy	**Major alloying element**
1xxx	Aluminium > 99%
2xxx	Copper
3xxx	Manganese
4xxx	Silicon
5xxx	Magnesium
6xxx	Magnesium and silicon
7xxx	Zinc
8xxx	Other

of the car body. The outer panels, where surface appearance is very important, are mainly made of aluminium-magnesium-silicon alloys (AA 6xxx alloys) which are less deformable but do have a good surface quality [3].

Since producing aluminium from aluminium ore costs about ten times more energy than recycling aluminium, it is economically attractive to recycle aluminium. Hence it would be preferable to use only one alloy type for the car bodies, which makes it easier to recycle.

1.3 Metal forming

In metal forming, a piece of metal is plastically deformed between tools in order to obtain a certain shape. Typical forming processes are rolling, forging, deep drawing, extrusion and hydroforming.

Car body panels are usually manufactured by deep drawing. In this process a product is made of sheet metal. An initially flat blank is clamped between a die and a blank holder. Next a punch moves down to deform the clamped blank into the desired shape, as illustrated in Figure 1.2.

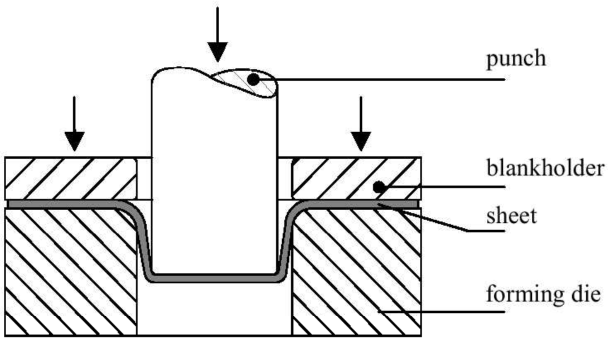

Figure 1.2: Schematic representation of the deep drawing process

The final shape of the product depends on the geometry of the tools, the material behaviour of the blank and the process parameters. For instance, the formability of aluminium can be increased significantly by elevating the process temperature. It is shown that the limiting drawing ratio of an AA 5754-O alloy cup can be increased from 2.1 to 2.6 by heating the flange up to 250 °C and cooling the punch to room temperature [4,18]. This gives an increase in maximum attainable cup height of 70 %, as illustrated in Figure 1.3. An additional advantage is that stretcher lines do not appear when AA 5xxx alloys are deformed at elevated temperatures.

Figure 1.3: Increased maximum cup height achieved with the flange at 250° C (courtesy of TNO Eindhoven)

1.4 Numerical simulations

In industry there is not much experience in processing aluminium sheet at elevated temperatures. Since trial and error in the workshop is very expensive, it is important to use numerical simulations to predict and optimise the deep drawing process.

For accurate simulation of any forming process it is necessary that the material behaviour is known. Therefore a proper material model that describes the relation between stress, strain, strain rate and temperature for aluminium when it is deformed at elevated temperatures is required.

The purpose of this graduation project is to develop a material model for aluminium that takes variations in temperature and strain rate into account. Constant strain rate tests have been conducted at TNO Eindhoven for strain rates of $0.002\,\mathrm{s}^{-1}$, $0.02\,\mathrm{s}^{-1}$ and $0.1\,\mathrm{s}^{-1}$ and temperatures between $25\,°\mathrm{C}$ and $250\,°\mathrm{C}$. The results of these tests have been used to determine the parameters of two different material models. One of these material models is applied in a finite element program.

1.5 Outline of the thesis

In Chapter 2 the theoretical background for this project is described. First some basic theory is explained. Subsequently a phenomenological and a physically based method to model the behaviour of aluminium at elevated temperatures are given.

Constant strain rate tests on an AA 5754-O alloy have been performed on a mechanical tensile testing machine at TNO Eindhoven. In Chapter 3 these tensile tests are described and used to determine the parameters of both material models described in Chapter 2. With one of these models numerical simulations of a tensile test have been performed. The results of these simulations can be found in Chapter 4.

To determine which material model describes the behaviour of aluminium during a rapid change in strain rate (a strain rate jump) at elevated temperatures best, more tensile tests have been performed on a hydraulic tensile testing machine at the University of Twente. In Chapter 5 these uniaxial tensile tests with strain rate jumps are described.

Finally in Chapter 6 the conclusions from this research are summarised and recommendations for future research are presented.

Chapter 2

Modelling material behaviour

In this chapter the theory used in this thesis is presented. First the basic relationship between stress and strain is given. Next the influence of temperature and strain rate on this stress-strain relationship is described. Finally both a phenomenological and a physically based material model that are used to model the material behaviour of aluminium at elevated temperatures are presented.

2.1 Stress and strain

The relationship between stress and strain of a material can be determined in a tensile test. This is one of the most commonly used tests for evaluating material behaviour. A test specimen is loaded uniaxially, resulting in a gradual elongation and eventually fracture of the specimen. The measured tensile force F and displacement $\Delta L = L - L_0$ are used to calculate the engineering stress S and the engineering strain e:

$$S = \frac{F}{A_0} \tag{2.1}$$

$$e = \frac{L - L_0}{L_0} \tag{2.2}$$

with A_0 the initial cross-sectional area, L the current length and L_0 the initial length. In Figure 2.1 a typical engineering stress-strain curve produced in a uniaxial tensile test is given.

The engineering stress and strain depend on the initial length and cross-sectional area of the specimen. When the results of the tensile tests are used to predict how the material will behave under other conditions, it is desirable to translate the results to the true stress σ and true strain ε. True stress is defined as:

$$\sigma = \frac{F}{A} \tag{2.3}$$

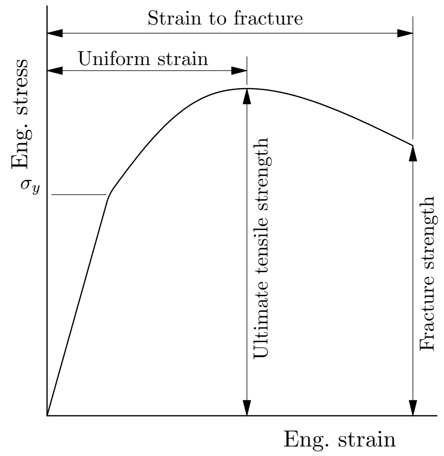

Figure 2.1: A typical engineering stress-strain curve

with A the current cross-sectional area. Up to the point at which necking starts, true strain is defined as:

$$\varepsilon = \ln \frac{L}{L_0} \tag{2.4}$$

As long as the deformation is uniform along the gauge section the true stress and strain can be calculated from the engineering stress and strain, assuming constant volume:

$$\sigma = S(1 + e) \tag{2.5}$$

$$\varepsilon = \ln(1 + e) \tag{2.6}$$

2.1.1 Elastic deformation

At small stresses only elastic deformation occurs. The bonds between atoms are stretched and when the stress is removed, the bonds relax and the material returns to its original shape. This reversible deformation is characterised by a linear relation between stress and strain and is described by Hooke's law for elasticity:

$$\sigma = E\varepsilon \tag{2.7}$$

with E the Young's modulus of the material.

2.1.2 Plastic deformation

The yield strength σ_y gives the level of stress above which plastic deformation occurs and is usually defined as the stress after 0.2% plastic strain.

The flow stress σ_f denotes the resistance to plastic deformation of a material. As a ductile material is plastically deformed it becomes harder and stronger, a process known as strain hardening. Strain hardening can be explained on the basis of interactions between dislocations. When a material is being deformed, the dislocation density increases. Consequently the average distance between dislocations decreases and the motion of a dislocation is hindered by the presence of other dislocations. As the dislocation density increases, the resistance to dislocation motion by other dislocations becomes more pronounced and the stress necessary to deform a metal increases.

The relation between flow stress and strain is often described by a power law, e.g. the Nadai relation:

$$\sigma_f = C_1 \varepsilon^n \tag{2.8}$$

with C_1 a material constant and n the strain hardening coefficient, which gives an indication of the ability of the sheet to distribute the strain over a wide region [9, 12].

2.2 Temperature and strain rate effects

The relationship between stress and strain also depends on the strain rate $\dot{\varepsilon}$ and temperature T. Stress-strain curves of most metals and alloys decrease as the strain rate decreases or as the temperature increases. This strain rate and temperature dependence is illustrated in Figure 2.2. Since the formability of a material depends on the deformation process, the strain rate and the temperature, the formability of aluminium for a specific deformation process can be improved by optimising both the strain rate and the temperature of that process.

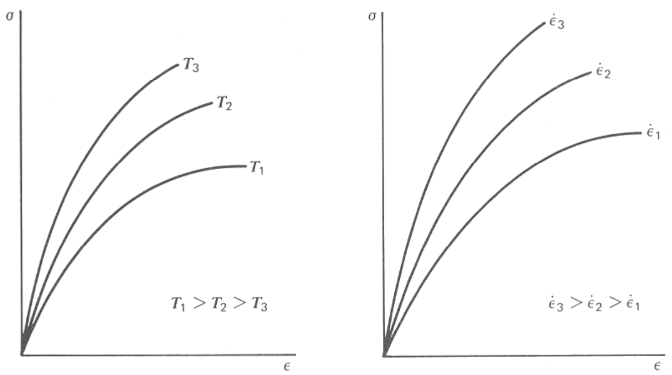

(a) Temperature effects (b) Strain rate effects

Figure 2.2: The influence of temperature and strain rate on stress-strain curve [10]

2.2.1 Temperature effects

The melting temperature of aluminium-magnesium alloys is in the order of 640 °C. The homologous temperature T_h is defined as the absolute temperature T^a divided by the absolute melting temperature T^a_m:

$$T_h = \frac{T^a}{T^a_m} \tag{2.9}$$

For the temperature range of interest for this research (25 °C to 250 °C), the homologous temperature ranges from 0.33 to 0.57. At homologous temperatures between 0.3 and 0.5, the material strength decreases because of thermally activated processes like cross slip that allow the high local stresses to be relaxed. For higher temperatures, diffusion processes become important and mechanisms like recovery and recrystallisation prevent pile-ups and further reduce the strength of the material.

Recovery is the relieve of the build-up of dislocations from strain hardening when crystal imperfections are rearranged or eliminated into new configurations. For AA 5xxx alloys recovery can already start at temperatures as low as $95 - 120$ °C.

Recrystallisation is a rapid restoration process, in which new, dislocation-free crystals nucleate and grow at the expense of original grains. For AA 5xxx alloys recrystallisation occurs only above 250 °C so it is not expected to occur during the tensile tests performed for this project [5, 9, 12].

2.2.2 Strain rate effects

The relationship between stress and strain rate for a certain strain and temperature is often described by a power-law of the same form as Equation 2.8:

$$\sigma = C_2 \dot{\varepsilon}^m \tag{2.10}$$

with C_2 a material constant and m the strain rate sensitivity. For most metals m varies between 0.02 and 0.2. The strain rate sensitivity increases with increasing temperatures.

2.2.3 Dynamic strain ageing

In a tensile test at room temperature the AA 5xxx alloys show serrated flow curves, which is illustrated in Figure 2.3. This behaviour is known as the Portevin-LeChatelier effect and is attributed to dynamic strain ageing. In deep drawing this effect can lead to stretcher lines in a product, which results in a poor surface quality [9].

A physical explanation for dynamic strain ageing can be found in the interaction between dislocations and solute atoms. The solute magnesium atoms obstruct dislocation movement, which leads to a higher initial yield strength.

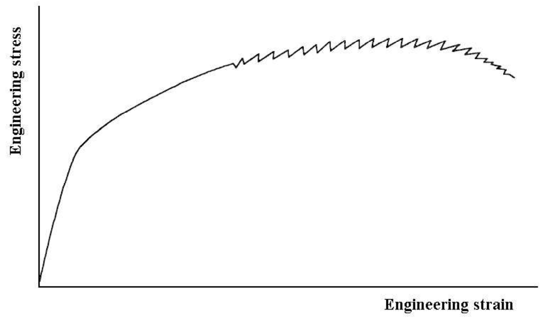

Figure 2.3: Serrated flow curve [9]

At low strain rates dislocations move slowly and the solute atoms can migrate to the dislocation while they are arrested at other obstacles or solute atoms. This further obstructs dislocation movement and causes a higher flow stress. At higher strain rates the solute atoms cannot migrate to the dislocations, which results in a lower flow stress. Macroscopically this appears as a negative strain rate sensitivity, which can lead to instabilities.

At elevated temperatures the mobility of the solute atoms increases and the serrations disappear. Therefore, when forming at elevated temperatures no stretcher lines occur, and the surface quality is good [9, 18].

2.3 Material models

There are several ways to model material behaviour. In this section two models are presented: a phenomenological and a physically based material model. Both models describe the flow stress as a function of the deformation path, temperature and strain rate.

2.3.1 A phenomenological model

A phenomenological model is actually the classical approach for modelling material behaviour. Macroscopic mechanical test results are fitted to a convenient mathematical function. A good approximation of the stress-strain curve was already given in Equation 2.8. If the material is pre-strained the relationship changes to:

$$\sigma = C_1(\varepsilon + \varepsilon_0)^n \tag{2.11}$$

with ε_0 the initial strain.

This equation only considers strain hardening. In Section 2.2 it was shown that the strain rate and temperature also have a significant influence on the stress. The strain rate sensitivity is described in Equation 2.10.

Combining Equations 2.10 and 2.11 gives:

$$\sigma_f = C(\varepsilon + \varepsilon_0)^n \left(\frac{\dot{\varepsilon}}{\dot{\varepsilon_0}}\right)^m \tag{2.12}$$

with $\dot{\varepsilon_0}$ a reference strain rate.

The effect of the temperature on the stress is accounted for by assuming that C, n and m are functions of the temperature. The following relations were shown to give good results [20]:

$$C(T) = C_0 + a_1 \left[1 - \exp\left(a_2 \frac{T - 273}{T_m}\right)\right] \tag{2.13}$$

$$n(T) = n_0 + b_1 \left[1 - \exp\left(b_2 \frac{T - 273}{T_m}\right)\right] \tag{2.14}$$

$$m(T) = m_0 \exp\left(c \frac{T - 273}{T_m}\right) \tag{2.15}$$

with C_0, a_1, a_2, n_0, b_1, b_2, m_0 and c material constants and T_m a reference temperature. From now on this model will be referred to as the extended Nadai model [18–20].

2.3.2 A physically based material model

A physically based model predicts the relationship between stress and strain by considering the physical mechanisms of plastic deformation. The physically based model used here was first described by Bergström [1,2] and has been adapted by Van Liempt [21]. The deformation resistance of metals is divided into three parts:

$$\sigma_f = \sigma_o(T) + \sigma_w(\rho, T) + \sigma^*(\dot{\varepsilon}, T) \tag{2.16}$$

with σ_0 the strain rate independent stress, σ_w the contribution of the strain hardening and σ^* a dynamic stress that depends on the strain rate and temperature.

Dynamic stress

The dynamic stress σ^* is often defined by a relation attributed to Krabiell and Dahl [11]:

$$\begin{gathered}\sigma^*(\dot{\varepsilon}, T) = \sigma_0^* \left\{1 + \frac{kT}{\Delta G_0} \ln\left(\frac{\dot{\varepsilon}}{\dot{\varepsilon_0}}\right)\right\} \\ \text{for} \quad \dot{\varepsilon}_0 \exp\left(-\frac{\Delta G_0}{kT}\right) < \dot{\varepsilon} < \dot{\varepsilon}_0\end{gathered} \tag{2.17}$$

with σ_0^* a maximum value for the dynamic stress, k the Boltzmann's constant and ΔG_0 the activation energy.

The preliminary results of the tensile tests performed at TNO Eindhoven show that the influence on the initial yield stress is small at low temperatures and increases rapidly at higher temperatures [19, 20]. However, Equation 2.17 gives a high strain rate influence at low temperatures that decreases at high temperatures. Since this is in contradiction to the experimental results, the dynamic stress neglected.

Strain hardening

For the contribution of strain hardening σ_w, a simple one-parameter model is used where the evolution of the dislocation density ρ is responsible for the hardening. The relation between the dislocation density and the strain hardening is given by the Taylor equation:

$$\sigma_w = \alpha G(T) b \sqrt{\rho} \tag{2.18}$$

with α a scaling parameter, G the elastic shear modulus and b the Burgers vector [18].

The essential part of Equation 2.18 is the evolution of the dislocation density. This gives the influence of temperature and strain rate on the hardening. It is formulated as an evolution equation:

$$\frac{d\rho}{d\varepsilon} = U(\rho) - \Omega(\dot{\varepsilon}, T)\rho \tag{2.19}$$

with U the immobilisation rate of dislocations and Ω the remobilisation rate of dislocations:

$$U = U_0 \sqrt{\rho} \tag{2.20}$$

$$\Omega = \Omega_0 + C_3 \mathrm{exp}\Big(- \frac{mQ_v}{RT} \Big) \dot{\varepsilon}^{-m} \tag{2.21}$$

with U_0 the intrinsic immobilisation rate, Ω_0 the low temperature, high strain rate limit value of the remobilisation probability, C_3 and m constants, Q_v the activation energy and R the gas constant.

Equation 2.19 can be integrated analytically for constant U_0 and Ω [8, 21]. For an incremental algorithm, the dislocation density ρ_{i+1} at time t_{i+1} can be calculated from:

$$\rho_{i+1} = \left[\frac{U_0}{\Omega} \Big(\exp(\tfrac{1}{2}\Omega\Delta\varepsilon) - 1 \Big) + \sqrt{\rho_i} \right]^2 \exp(-\Omega\Delta\varepsilon) \tag{2.22}$$

where U_0 and Ω are assumed to be constant during the time increment. This gives a contribution to the flow stress of:

$$\sigma^w_{i+1} = \alpha G b \sqrt{\rho_{i+1}} \tag{2.23}$$

which leads to:

$$\sigma^w_{i+1} = \alpha G b \left[\Big(\frac{U_0}{\Omega} - \sqrt{\rho_i} \Big) \Big(1 - \exp(-\tfrac{1}{2}\Omega\Delta\varepsilon) \Big) + \sqrt{\rho_i} \right] \tag{2.24}$$

Strain rate independent stress

The strain rate independent stress σ_0 is assumed to relate to stresses in the atomic lattice. Therefore the temperature dependence of the shear modulus $G(T)$ is also used for the strain rate independent stress [16, 18].

Bergström model

Combining Equation 2.16 with the information described above results in:

$$\sigma_f = g(T)\Big(\sigma_0 + \alpha G_{ref} b\sqrt{\rho}\Big) \tag{2.25}$$

with $g(T)$ the shear modulus divided by the reference value G_{ref}. In this work the temperature dependence is numerically represented by the empirical relation:

$$g(T) = 1 - C_T \exp\left(-\frac{T_1}{T}\right) \tag{2.26}$$

with C_T and T_1 fitting parameters. From now on this model will be referred to as the Bergström model.

Chapter 3

Experiments at constant strain rate

Constant strain rate tensile tests have been performed at TNO Eindhoven. In this chapter these tests and the results are first described. After this the parameters of the material models described in Chapter 2 are determined using these tensile test results. The objective is to predict the behaviour of aluminium-magnesium alloys when deformed at elevated temperatures.

3.1 Tensile testing at TNO Eindhoven

In this section the tensile tests that were performed at TNO Eindhoven are described. First the characteristics of the tested material and the experimental test set-up are discussed. Subsequently the results of the performed tensile tests are given.

3.1.1 Material characteristics of 5754-O

In this thesis, the AA 5754-O alloy is used for the experiments as a representative example of the 5xxx alloys. The chemical composition of this alloy, as given by the manufacturer, is presented in Table 3.1. The main alloying element is magnesium, which has a strengthening effect on the aluminium. Since the solid solubility of this alloying element is higher than 10 %, it is in solid solution and the alloy constitutes of a single phase. This means that the original crystal structure of the aluminium is maintained. The mean grain size of the alloy is $20 - 25\,\mu$m.

The AA 5754-O alloy is in a fully annealed state. Therefore the test results are not influenced by the time that a specimen is kept at elevated temperatures prior to deformation.

The test specimens were manufactured according to EN-10002 Form 1, as illustrated

Table 3.1: The chemical composition of the AA 5754-O alloy

Alloying element	%
Magnesium	3.356
Manganese	0.320
Silicon	0.130
Copper	0.010
Titanium	0.009
Aluminium	Remainder

in Figure 3.1. They were made from a single batch of sheet material with a thickness of 1.2 mm. The tensile direction is perpendicular to the rolling direction of the sheet material. The elongation of the specimen during testing is measured directly over an initial length of 50 mm.

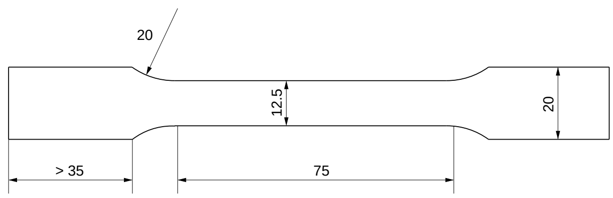

Figure 3.1: Tensile test specimen according to EN-10002 Form 1 (dimensions in mm)

3.1.2 Experimental set-up

All tests were performed on a Zwick mechanical tensile tester. Prior to testing the specimen and clamps were placed in a furnace. The furnace was heated to the desired temperature, after which the specimen was clamped on one side. After re-heating the furnace, the other side was clamped. The test was started when the desired testing temperature was reached again. Depending on the required temperature, it took about one to three minutes before the specimen was clamped properly and the test could be started. The temperature in the furnace was controlled by a PID controller within 1 °C.

3.1.3 Tensile test results

Tensile tests at a constant strain rate and constant temperature were conducted at various strain rates ($0.002\,\mathrm{s}^{-1}$, $0.02\,\mathrm{s}^{-1}$ and $0.1\,\mathrm{s}^{-1}$) and temperatures (between room temperature and 250 °C). Per strain rate and temperature, two to five tests have been performed. The experiments were conducted over a time-span of one year, but no systematic difference between test results was found.

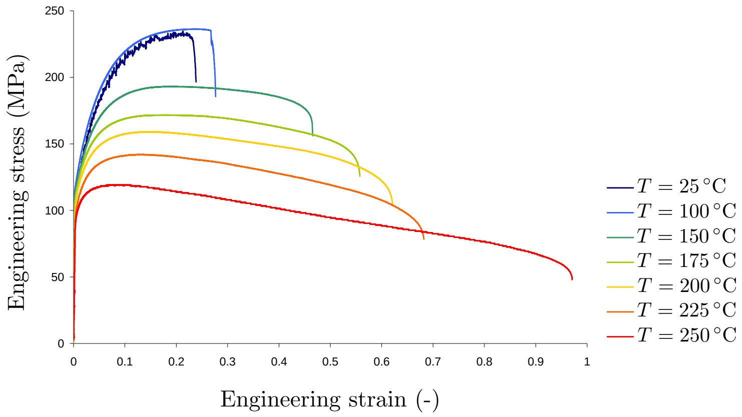

(a) $\dot{\varepsilon}$ =0.002s^{-1}

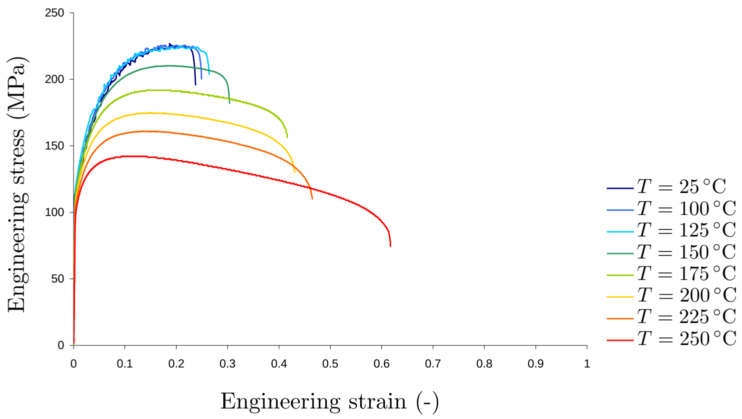

(b) $\dot{\varepsilon}$ =0.02s^{-1}

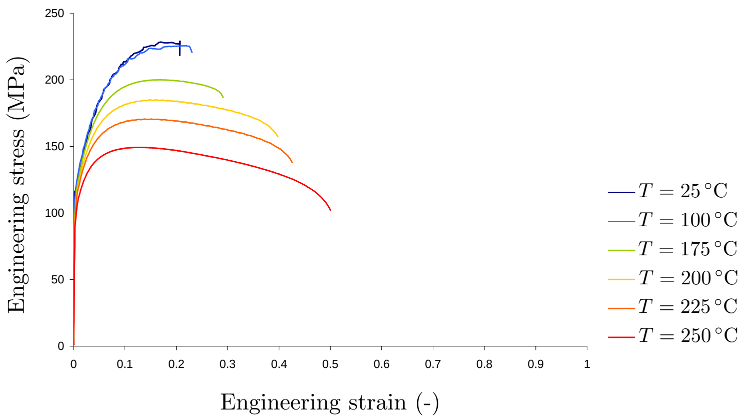

(c) $\dot{\varepsilon}$ =0.1s^{-1}

Figure 3.2: Temperature influence on engineering stress-strain curves

In Figure 3.2 the temperature influence on the engineering stress-strain curves can be seen. Only one representative result per specific test is given. The stress-strain curves at relatively low temperatures show the serrations that cause the stretcher lines, as explained in Section 2.2.3. Figure 3.2(b) shows that for temperatures above 125 °C these serrations no longer occur. For all strain rates there is hardly any difference between the stress-strain curves at room temperature and at 100 °C. When the test temperature exceeds 125 °C, the ultimate tensile strength decreases with increasing temperature.

In Figure 3.3 the stress-strain curves are plotted per temperature. From this the strain rate sensitivity of the AA 5754-O alloy can be clearly seen. At the lower temperatures the lowest strain rate gives the highest stresses, see Figures 3.3(a) and 3.3(b). This is often presented as a negative strain rate sensitivity and is attributed to dynamic strain ageing. At higher temperatures the stress-strain curves show the more common situation that with increasing strain rate the stress increases and the strain to fracture decreases.

3.2 Determination of material parameters

In this section the experimental results are used to determine the parameters of the material models described in Section 2.3. First the procedure is explained and subsequently the results for both the extended Nadai and the Bergström model are given. Finally a comparison between the fitted models and the experiments is presented.

3.2.1 Optimisation

Optimisation techniques are used to find a set of design variables that can in some way be defined as optimal. In this case the design variables are the parameters of the two material models described in Section 2.3 and optimal means that the difference between the stress-strain curves given by the tensile tests performed at TNO and the stress-strain curves given by the material models should be as small as possible.

Only the part between the yield stress and the ultimate tensile strength is fitted to the material model. The elastic part of the stress-strain curve has been neglected, because it is only a small part of the total strain. After the point where necking occurs, the strain is no uniform anymore. Therefore that part of the stress-strain curve is neither used for fitting the material models.

To fit the material models to the experimental data a least square approximation was used. This means that the function to be minimised was expressed as:

$$f(x) = \int_{t_1}^{t_2} (y(x,t) - \phi(t))^2 dt \tag{3.1}$$

with t a scalar, y the function for the material model, which depends on the vector x and ϕ the experimental data.

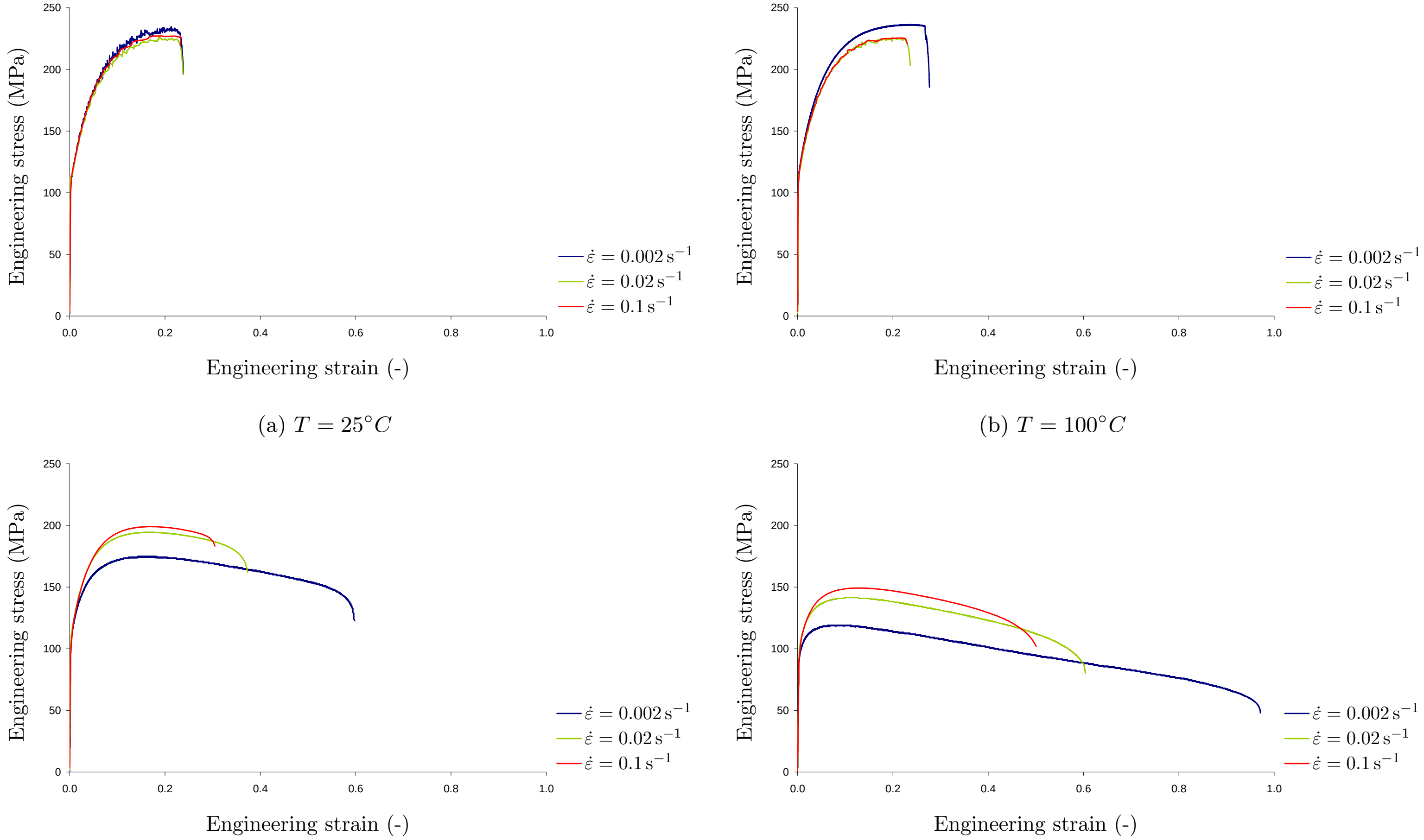

(a) $T = 25°C$

(b) $T = 100°C$

(c) $T = 175°C$

(d) $T = 250°C$

Figure 3.3: Strain rate influence on engineering stress-strain curves

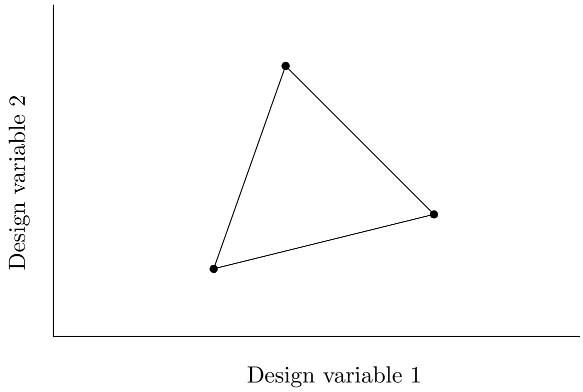

Figure 3.4: A simplex in 2 dimensions

For the minimising of this function an unconstrained minimisation technique was used: the simplex search of Nelder and Mead [14]. This is a direct search method that only uses function evaluations without applying numerical or analytical gradients.

Simplex search methods are based on an initial design of n+1 trials, where n is the number of variables. A simplex is an n+1 geometric figure in an n-dimensional space. In Figure 3.4 a simplex in a 2-dimensional space is given, hence the simplex is a triangle. The corners of the geometric figure are called vertices and the simplex search method evaluates the function at each vertex. It then decides which is the worst value and mirrors that vertex through the centroid of the remaining n vertices, thus forming a new simplex. The Nelder-Mead simplex search method has the additional advantage that it can adjust its shape and size depending on the response in each step. Therefore it is possible to accelerate the optimisation process.

Prior to fitting, the experimental data set was reduced to twelve stress-strain curves, each composed of 21 data points. Each stress-strain curve represents a single combination of the following temperatures and strain rates: 25 °C, 100 °C, 175 °C and 250 °C and $0.002\,\mathrm{s}^{-1}$, $0.02\,\mathrm{s}^{-1}$ and $0.1\,\mathrm{s}^{-1}$.

3.2.2 Extended Nadai model

The extended Nadai model has been described in Section 2.3.1. The parameters T_m and $\dot{\varepsilon}_0$ are used to scale parts of the equations, resulting in dimensionless expressions, and can be chosen arbitrarily. The remaining nine parameters were simultaneously fitted to the selected uniaxial tensile tests. In Table 3.2 the results of this fit are given. The standard deviation of the difference between the experimental results and the results given by the extended Nadai model, the so-called RMS error value, is 5.56 MPa.

Table 3.2: Parameters for the extended Nadai model

T_m	800 K	a_1	109.7 MPa	n_0	0.3212
ϵ_0	0.004603	a_2	3.965	m_0	0.001625
$\dot{\epsilon}_0$	0.002 s^{-1}	b_1	0.2389	c	10.23
C_0	488.0 MPa	b_2	1.463		

3.2.3 Bergström model

The Bergström model was described in Section 2.3.2. Some of the parameters in this model can be selected beforehand. The initial dislocation density ρ_0 was chosen to be $10^{11}\,m^{-2}$, which is a reasonable value for annealed aluminium. The magnitude of the Burgers vector b and the shear modulus at room temperature G_{ref} were taken from literature. Furthermore the scaling factor α was chosen to be 1.

The eight remaining parameters were fitted to the same tensile tests that were used to fit the extended Nadai model. In Table 3.3 the resulting values are presented. The RMS error value between the experimental results and the Bergström model is 3.76 MPa.

Table 3.3: Parameters for the Bergström model

σ_0	103.7 MPa	m	0.3456	ρ_0	$10^{11}\,m^{-2}$
α	1.0	U_0	$6.331 \cdot 10^8\,m^{-1}$	G_{ref}	26354 MPa
b	$2.857 \cdot 10^{-10}$ m	Ω_0	25.35	C_T	123.4
C	$3.232 \cdot 10^5$	Q_v	$1.287 \cdot 10^5$ J/mol	T_1	3639 K

3.2.4 Comparison of the models

In Figure 3.5 the simulated engineering stress-strain curves for both models are plotted together with the experimental data. Only the part of the curve that was used to fit the parameters is plotted. It can be seen that both models are capable of describing the experimental results. Since the RMS error value for the Bergström model (3.76 MPa) is less than the RMS error value for the extended Nadai model (5.56 MPa), the Bergström model gives a better fit. The difference between the models occurs mainly for $\dot{\varepsilon} = 0.002\,s^{-1}$, see Figure 3.5(a). For $T = 100\,°C$ the flow stress as given by the extended Nadai model is too low, while at $T = 175\,°C$ the flow stress is overestimated. In Chapter 4 the Bergström model will be used for numerical simulations of the tensile tests conducted at TNO Eindhoven.

When predicting the material behaviour at constant strain rates and constant temperatures both models give more or less the same results. However, the two material

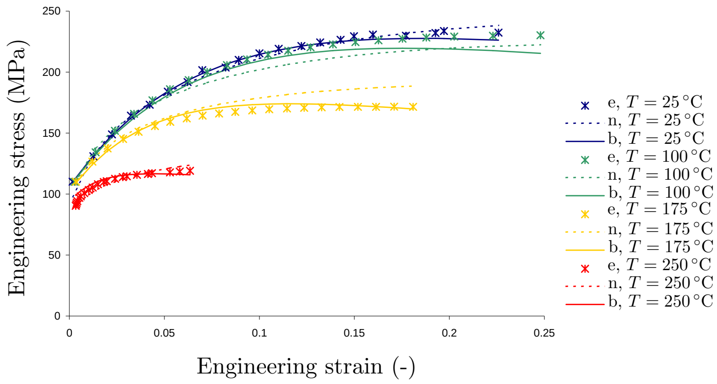

(a) $\dot{\varepsilon}$ =0.002s^{-1}

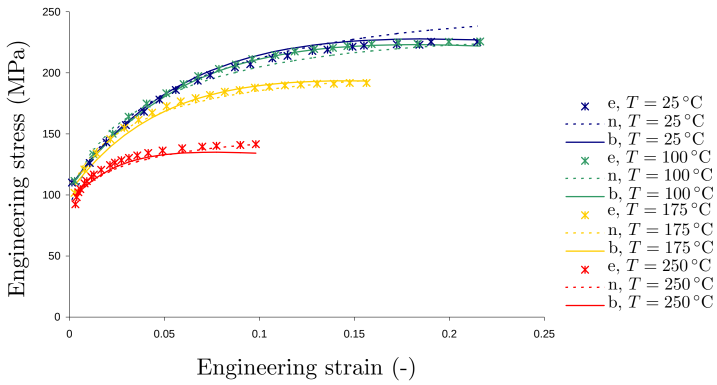

(b) $\dot{\varepsilon}$ =0.02s^{-1}

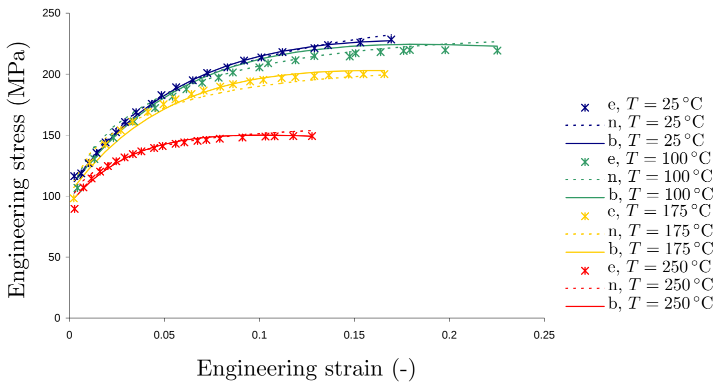

(c) $\dot{\varepsilon}$ =0.1s^{-1}

Figure 3.5: Engineering stress-strain curves for e = experiments, n = extended Nadai model and b = Bergström model

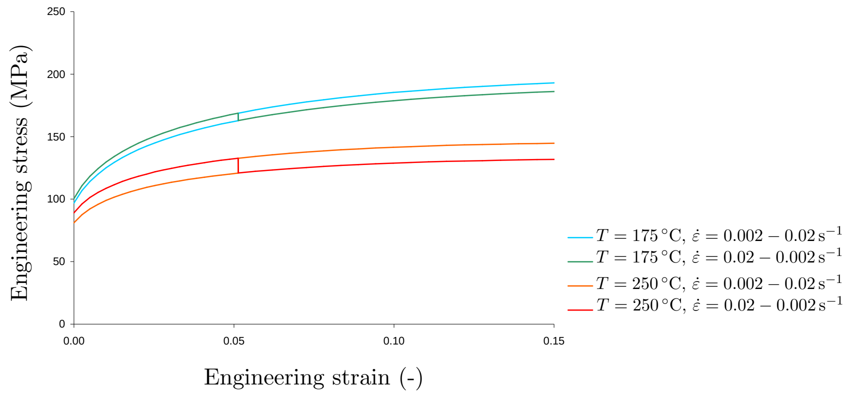

(a) Extended Nadai model

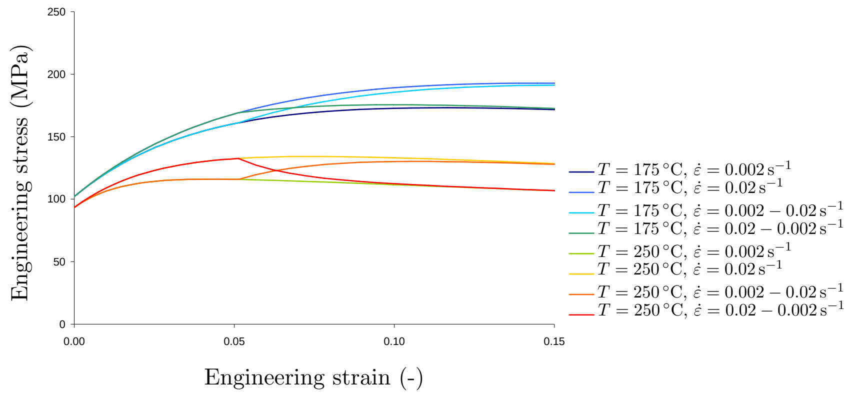

(b) Bergström model

Figure 3.6: Engineering stress-strain curves with and without strain rate jumps

models give completely different predictions when a jump in the strain rate is simulated. A jump in strain rate can be applied by altering the strain rate instantaneous at a certain strain. In Figure 3.6 stress-strain curves are plotted for deformation at $175\,°\mathrm{C}$ and $250\,°\mathrm{C}$ with strain rates $0.002\,\mathrm{s}^{-1}$ and $0.02\,\mathrm{s}^{-1}$. Strain rate changes from $0.002\,\mathrm{s}^{-1}$ to $0.02\,\mathrm{s}^{-1}$ or vice versa are applied after a strain of 0.05. It can be seen that the extended Nadai model immediately follows the curve of the other constant strain rate curve. The Bergström model only slowly approaches the other constant strain rate curve. To verify which of the two models predicts the material behaviour best, tests at constant temperature with strain rates jumps were performed at the University of Twente. In Chapter 5 these experiments and the results are described.

Chapter 4

Finite element simulations

In this chapter the applicability of the Bergström model is demonstrated by numerical simulations of uniaxial tensile tests. The finite element program used for the numerical simulations described in this chapter is called DiekA*. This program is being developed at the University of Twente and is specifically designed to simulate forming processes.*

4.1 Simulating tensile tests

The Bergström material model with the parameters as derived in Section 3.2.3 is applied in numerical simulations. The tensile test specimens used in the tensile tests performed at TNO Eindhoven, as described in Section 3.1.1, are modelled and meshed in the finite element program DiekA, see Figure 4.1(a). As the clamping area of the specimen is also modelled, a slight non-uniform strain distribution occurs which results in necking at the centre of the specimen, without prescribing an initial imperfection. In contrast to low temperatures, at elevated temperatures the tensile specimen necks perpendicular to the tensile direction. This results in a symmetric situation. Therefore it is only necessary to model a quarter section of the specimen and then specify symmetric conditions.

In order to describe necking accurately, the mesh is refined at the centre area. The smallest elements have a size of approximately 1 mm, which is of the same order as the sheet thickness. This necking can be seen in Figure 4.1(b) where a deformed mesh is given.

4.2 Results

Equivalent with the experimental results, the numerical stress-strain curves were determined for a gauge length of 50 mm. In Figure 4.2 both the numerical and experimental stress-strain curves are presented for strain rates of $0.002\,\mathrm{s}^{-1}$, $0.02\,\mathrm{s}^{-1}$ and

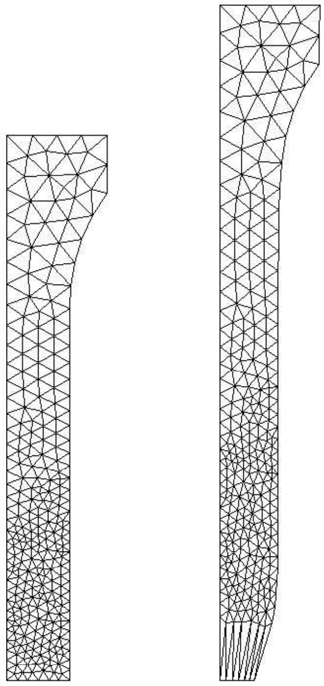

(a) (b)

Figure 4.1: Undeformed (a) and deformed (b) finite element meshes of a quarter of the tensile specimen

$0.1\,\mathrm{s}^{-1}$ and temperatures of 25 °C, 100 °C, 175 °C and 250 °C. Up to the ultimate stress the curves show a good resemblance. This is as expected, since the material parameters were determined using the experimental stress-strain data up to the ultimate tensile strength (uniform strain).

At the lower temperatures (25 °C and 100 °C) the calculated and experimental strain when the specimen fractures at localisation (when the specimen fractures) is nearly the same. At these temperatures, the strain rate does not have a large influence on the stress. For higher temperatures (175 °C and 250 °C) the simulated stress-strain curves follow the experimental stress-strain curves well after the ultimate tensile stress is reached. However, for the simulations localisation starts earlier than for the experiments.

Based on these results it can be concluded that the developed Bergström material model successfully describes the material behaviour of aluminium in uniaxial deformation at elevated temperatures and constant strain rates. The stress-strain curves are predicted accurately up to the ultimate tensile strength. After necking the numerical simulations have approximately the same softening slope as the experimental results, although localisation starts earlier.

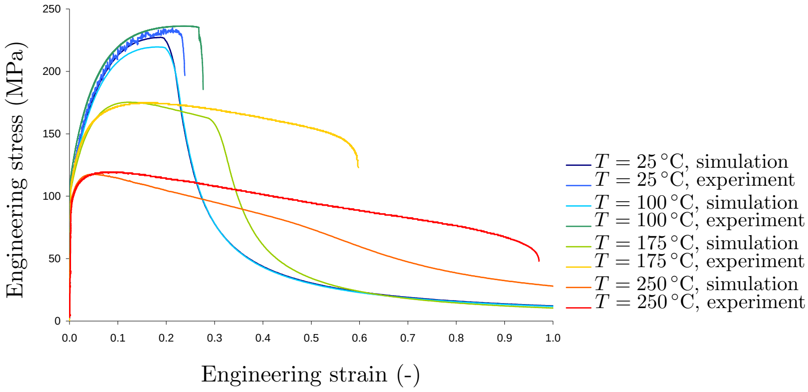

(a) $\dot{\varepsilon}$ =0.002s^{-1}

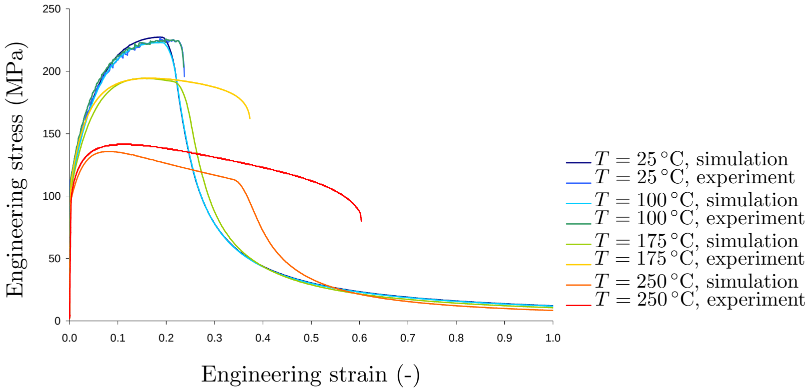

(b) $\dot{\varepsilon}$ =0.02s^{-1}

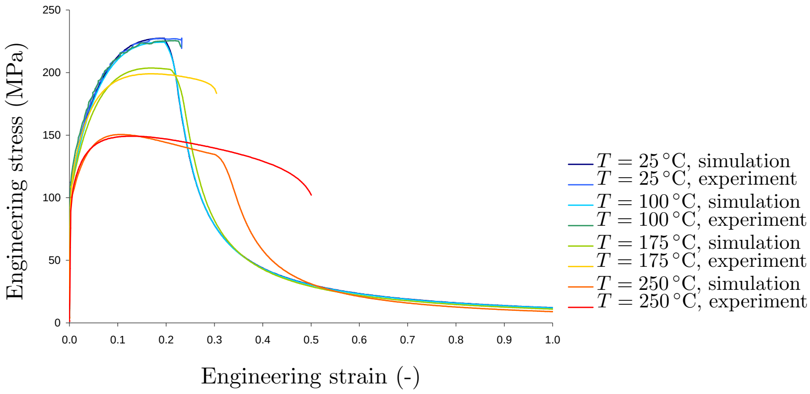

(c) $\dot{\varepsilon}$ =0.1s^{-1}

Figure 4.2: Stress-strain curves for simulations and experiments

In industrial applications, the strain rate is hardly ever constant. Therefore it is important to verify whether the material model describes the material behaviour correctly when a strain rate jump is applied. This verification is described in detail in Chapter 5.

Chapter 5

Experiments with a strain rate jump

Both material models described in Chapter 3 predict the material behaviour of aluminium at elevated temperatures and constant strain rates quite well. However there is a significant difference in the prediction of the material behaviour of both models in case a strain rate jump is applied. To verify which of the two models describes such a rapid change in strain rate correct, tensile tests with strain rate jumps at temperatures of 175°C and 250°C have been performed at the University of Twente. In this chapter the procedure and the results of these tests are described.

5.1 Experimental set-up

In this section the experimental test set-up of the experiments carried out at the University of Twente is first presented. Subsequently, the procedure to obtain the engineering stress and strain form the data-output is described.

5.1.1 Tensile test equipment

The tensile tests have been carried out on an Instron Model 8516 Testing System, which is a servo-hydraulic tensile testing system. The main advantage of this system, versus the mechanical system used at TNO, is that higher strain rates (over $\dot{\varepsilon} = 0.2\,\mathrm{s}^{-1}$) and faster strain rate jumps (from $\dot{\varepsilon} = 0.002\,\mathrm{s}^{-1}$ to $\dot{\varepsilon} = 0.02\,\mathrm{s}^{-1}$ within 0.1 s) are possible. In Figure 5.1 the used tensile test equipment is illustrated.

In these tensile tests the same aluminium-magnesium alloy (AA 5754-O) and specimens as applied in the TNO tests were used. To heat the specimens a tubular shaped furnace was used. Because it has a diameter of only 30 mm, special clamps were designed. To measure the temperature of the specimen during the test, a thermocouple

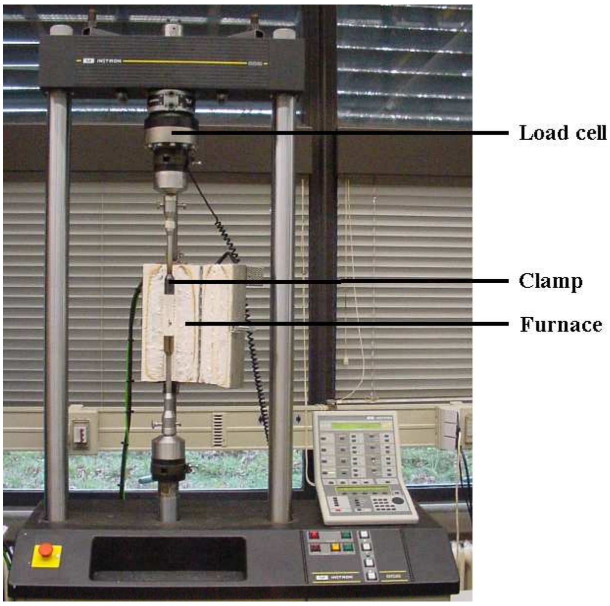

Figure 5.1: Experimental test equipment

was attached to the centre of the specimen. The temperature of the specimen, the force applied through the load cell and the displacement were all recorded. It was not possible to measure the strain of the specimen directly using a extensiometer, because of the limited space available in the furnace.

5.1.2 Determining the stress and strain

The engineering stress is calculated using Equation 2.1:

$$S = \frac{F}{A_0}$$

The initial cross-sectional area A_0 was calculated by multiplying the specimen thickness and width, which were measured for each specimen prior to testing using a screw gauge.

The engineering strain is calculated using Equation 2.2:

$$e = \frac{L - L_0}{L_0}$$

The strain is calculated from the measured displacement of the clamps. In the clamp area the strain is not completely uniform and therefore it is necessary to determine a representative initial length L_0 of the specimen. This length has been determined by a tensile test at room temperature. During this test an extensiometer with an initial gauge length of 50 mm was attached to the specimen. During the test both the displacement of the extensiometer and the displacement of the clamps were recorded. The result of this test is shown in Figure 5.2. It can be seen that the displacement of

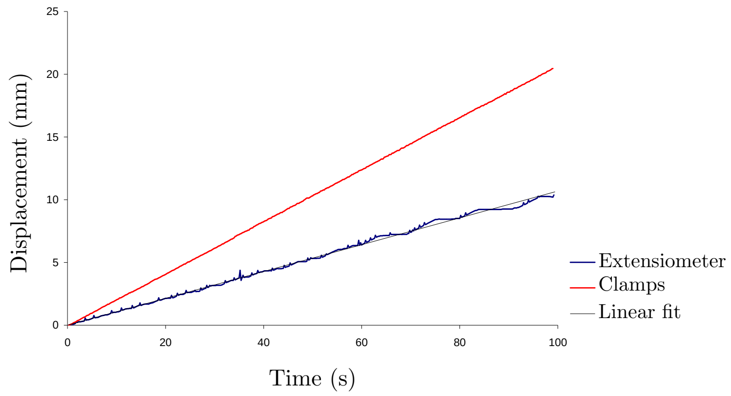

(a) Displacements of the extensiometer and the clamps

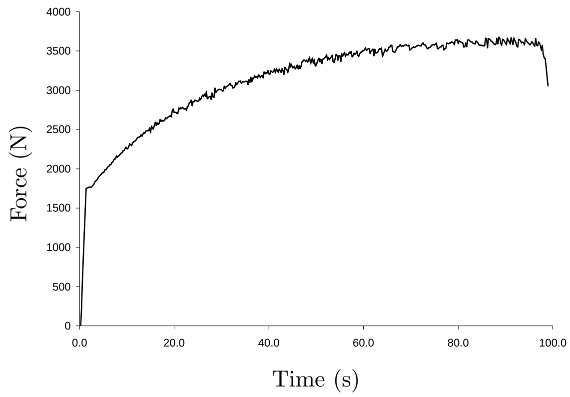

(b) Force-time curve

Figure 5.2: Tensile test at room temperature with $\dot{\varepsilon} = 0.002s^{-1}$

the clamps is linear with time. The displacement of the extensiometer is also fairly linear, but has some deviations, particularly towards the end of the curve where the force is almost maximal. This can be explained by stretcher lines that develop over the entire specimen, whereas the extensiometer only measures the elongation over a gauge length of 50 mm.

A linear trendline was fitted through the displacement of the extensiometer. When relating the slope of this line to the slope of the displacement of the clamps a representative initial gauge length L_{0c} can be calculated, knowing the initial gauge length of the extensiometer L_{0e}:

$$L_{0c} = L_{0e}\frac{\text{slope}_c}{\text{slope}_e} \approx 50\frac{0.2064}{0.1068} = 96.6\,\text{mm} \tag{5.1}$$

So instead of the actual initial gauge length of the specimen (which is 75 mm, see Figure 3.1) a representative initial gauge length of 96.6 mm is used to calculate the engineering strain.

5.2 Verification of the tensile tests

When conducting tensile tests it is important to know all factors that could influence the test results, like the test equipment used, the temperature distribution in the specimen and the heating of the specimen due to plastic deformation. In this section these factors are discussed.

5.2.1 Constant strain rate tensile tests

To correlate the results of the tensile tests performed at the University of Twente to the TNO results, first some tensile tests at elevated temperature were performed in which the strain rate was kept constant.

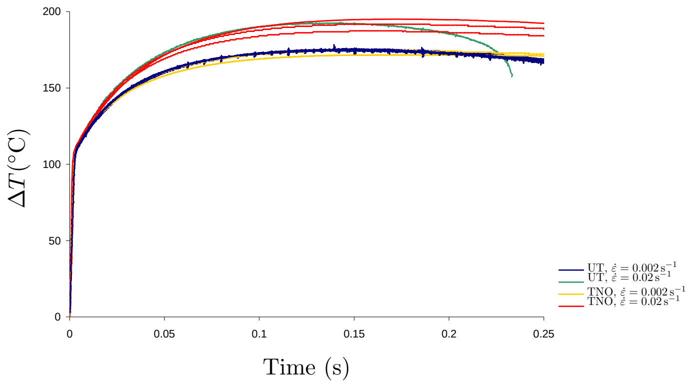

(a) $T = 175°C$

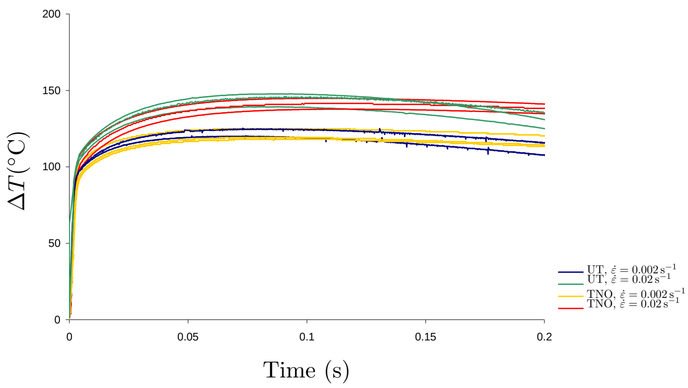

(b) $T = 250°C$

Figure 5.3: Comparison of tensile test results at a constant strain rate from the University of Twente (UT) and TNO Eindhoven (TNO)

In Figure 5.3 the results of these tests performed at the University of Twente are compared to the results of the tensile tests performed at TNO Eindhoven. It can be seen that for $\dot{\varepsilon} = 0.002\,\mathrm{s}^{-1}$ the results are quite similar up to uniform strain. Since the displacement of the specimen was not measured with the same initial gauge length, after uniform strain the results tests are not comparable anymore. For $\dot{\varepsilon} = 0.02\,\mathrm{s}^{-1}$ there is a larger difference between the stress-strain curves of the University of Twente and TNO. However, keeping in mind that the tests were performed on different tensile testers and individual tests also show a relatively large spread, these differences are acceptable.

5.2.2 Heating of a specimen

Prior to testing, the specimen is clamped in the tensile tester and the furnace is closed and turned on. It takes about 30 minutes before the specimen reaches a more or less steady state temperature of 175 °C or 250 °C. Since the furnace can only be turned on or off it is difficult to reach this testing temperature accurately. Therefore a temperature of 2-3 °C higher than the testing temperature was reached and the test was started when the specimen had cooled down to the testing temperature.

To verify whether the specimen is heated homogeneously in the furnace, tests have been performed with three thermocouples attached to the specimen, one in the centre and one at each end of the gauge. In Figure 5.4 the results for such a test are presented. In this case the specimen was heated to 250 °C, for tests where the specimen was heated to 175 °C similar results were obtained. When the furnace is turned on the specimen temperature rises. In Figure 5.4 it can be clearly seen that during the heating sequence the furnace was turned on and off six times. When the thermocouple attached to the centre of the specimen has reached the testing temperature, the tensile test is started. It can be seen that at this time ($t \approx 1700\,\mathrm{s}$) the upper thermocouple has approached approximately the same temperature. However the temperature of the lower thermocouple is about 18 °C lower. This difference in temperature can

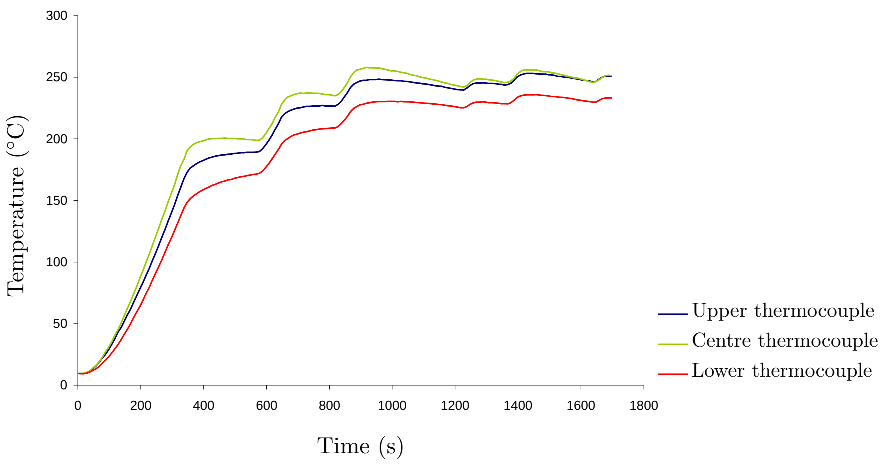

Figure 5.4: Heating of a specimen up to 250° C

be explained by the fact that the top and bottom of the furnace are not covered, resulting in an upward stream of cool air and a lower temperature in the lower half of the specimen.

It is not expected that the temperature gradient over the specimen influences the trend of the material behaviour, so the material behaviour in case of a strain rate jump can still be verified with the experiments. However for future testing it is recommended that the bottom and top of the furnace are covered to reduce the temperature gradient over the test specimen and the results of the tensile tests are more reliable.

5.2.3 Temperature rise during testing

During testing a tensile specimen can undergo an appreciable temperature rise. This is because most of the mechanical energy used to deform the specimen is converted into heat. The temperature rise of the specimen depends on the energy inserted by the test machine and on the amount of heat lost to the environment. If the test is rapid enough little heat is lost and the temperature rise can be surprisingly high. A high temperature rise in the specimen could have a significant influence on the measured properties, so it is important to know how much the temperature rises during the conducted tensile tests [9].

A first approximation of the temperature rise is available by assuming that the energy conversion process is adiabatic. In that case all the energy used for producing plastic deformation appears as heat. Assuming no heat is emitted to the environment, the temperature rise ΔT can be calculated with:

$$\Delta T = \frac{u}{c\rho} \tag{5.2}$$

With u the energy per volume, c the specific heat and ρ the density. For aluminium magnesium alloys $c = 960\,\mathrm{J/kgK}$ and $\rho = 2650\,\mathrm{kg/m^3}$ [17]. The energy per volume u is equal to the surface beneath the engineering stress-strain curve:

$$u = \int S \mathrm{d}e \tag{5.3}$$

In Figure 5.5 the (calculated) adiabatical and experimental temperature rise during two tensile tests and the difference between these two temperatures are given. Furthermore the rate of cooling was measured prior to the tensile test and a trend line for this cooling was extrapolated. In Figure 5.5(a) it can be seen that for low strain rates the difference between the theoretical and actual temperature rise is almost equal to the cooling trend line. The total temperature rise stays below 5 °C. For tests at higher strain rates, see Figure 5.5(b), there is not enough time for the specimen to cool down. Therefore the temperature rise of the specimen during testing is almost 20 °C. However, the ultimate tensile strength for tests at 250 °C is reached at a strain of 0.1. The temperature rise at this point is only 5 °C so the temperature rise is not expected to have a large influence for the stress-strain curves up to uniform strain.

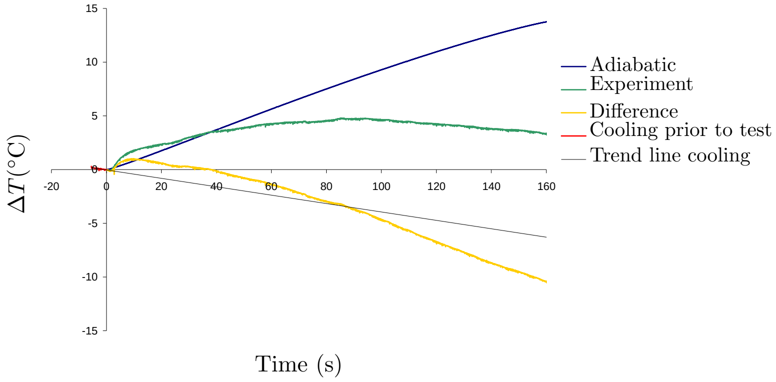

(a) $\dot{\varepsilon} = 0.002s^{-1}$

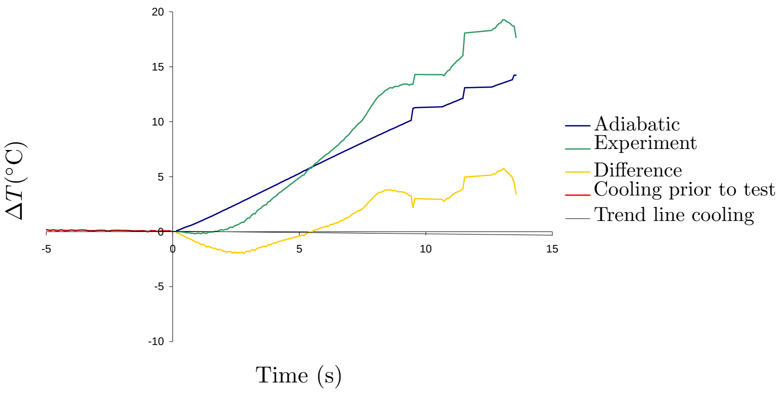

(b) $\dot{\varepsilon} = 0.02s^{-1}$

Figure 5.5: Theoretical and actual temperature rise of a specimen during tensile tests at $T = 250°\mathrm{C}$

5.3 Test results

In Figure 5.6 the experimental test results are presented. The different graphs show stress-strain curves at various temperatures and with various strain rates. Figures 5.6(a) and 5.6(b) give the results at $T = 175\,°\mathrm{C}$ with strain rates of $0.002\,\mathrm{s}^{-1}$ and $0.02\,\mathrm{s}^{-1}$. A jump in strain rate from the lower to the higher strain rate and vice versa is applied at a strain of 0.05 and 0.10. Figure 5.6(c) give the results at $T = 250\,°\mathrm{C}$ with strain rates of $0.002\,\mathrm{s}^{-1}$ and $0.02\,\mathrm{s}^{-1}$, in which the strain rate jumps are applied at a strain of 0.05. Figure 5.6(d) shows the same, but for a higher strain rate of $0.2\,\mathrm{s}^{-1}$.

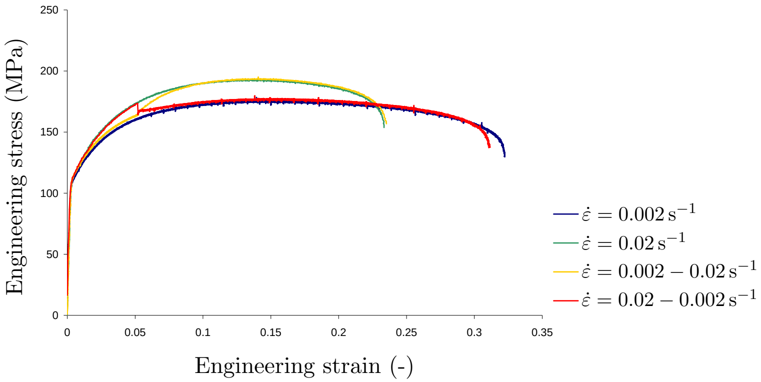

(a) $T = 175°C$

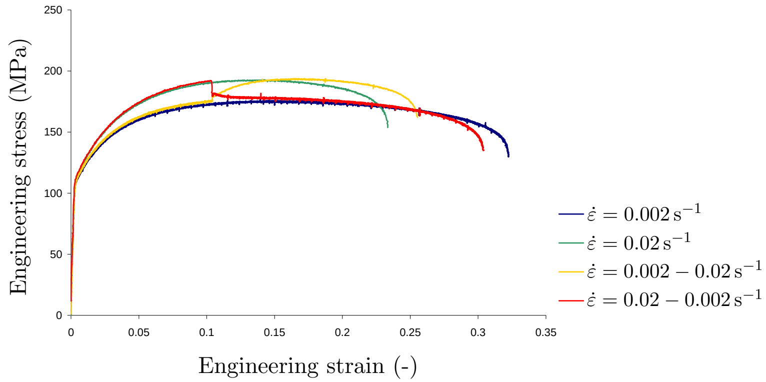

(b) $T = 175°C$

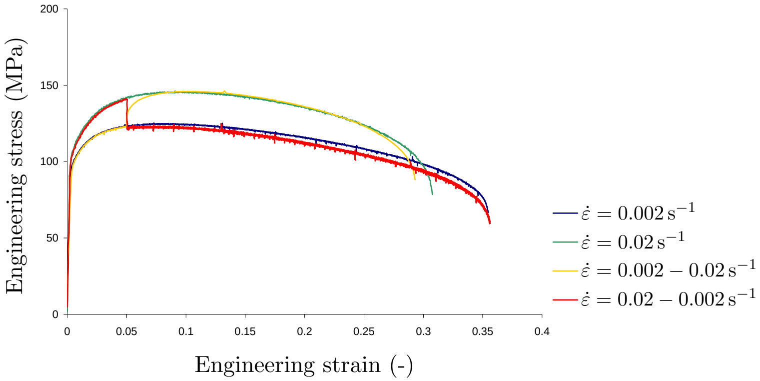

(c) $T = 250°C$

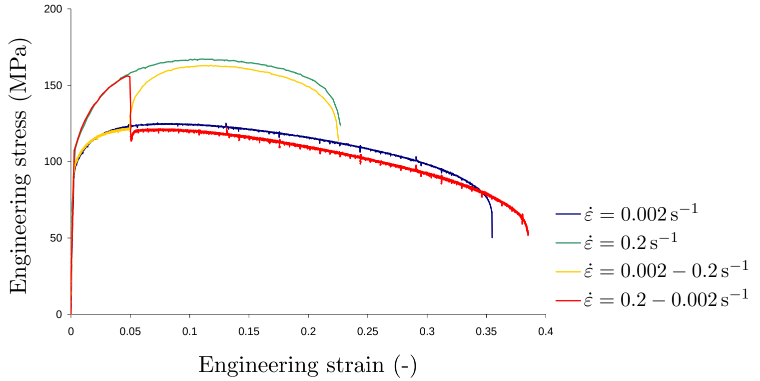

(d) $T = 250°C$

Figure 5.6: Experimental engineering stress-strain curves with strain rate jumps

When a strain rate jump is applied from a lower strain rate to a higher strain rate, it can be seen that the stress initially increases rapidly and then increases further at a lower rate until the curve that represents the test with the higher constant strain rate is reached. For the experiments conducted at 250 °C the instantaneous response is much larger than for the experiments conducted at 175 °C, which can be seen in Figure 5.7 more clearly.

When the strain rate decreases at 175 °C it can be seen that there is a rapid instantaneous decrease in stress, followed by a decrease at a lower rate until the curve that represents the constant strain rate test of $0.002\,\mathrm{s}^{-1}$ is reached. At 250 °C the stress drops immediately and no transient phenomenon is observed.

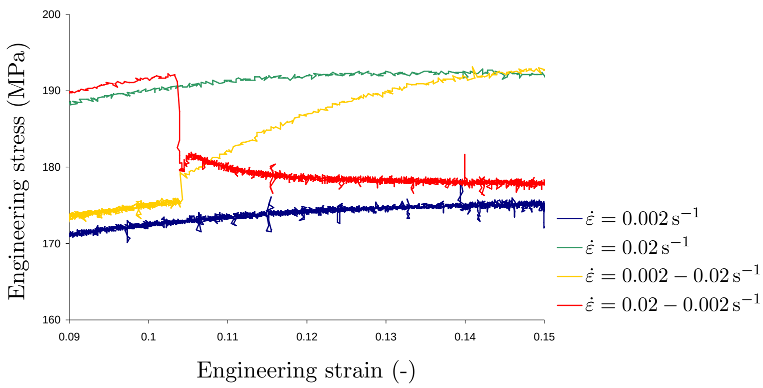

(a) $T = 175°C$

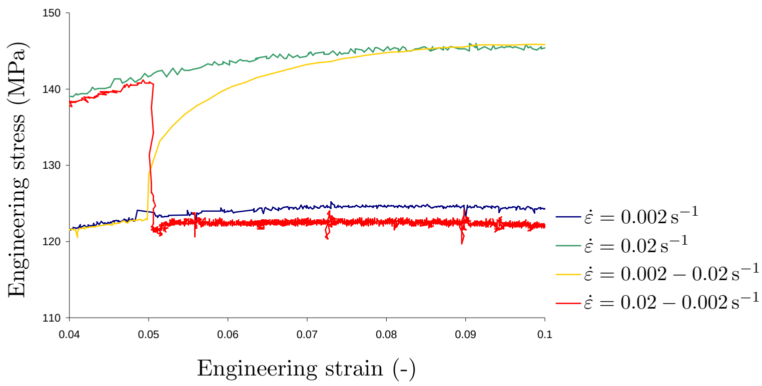

(b) $T = 250°C$

Figure 5.7: Experimental engineering stress-strain curves with strain rate jumps

5.4 Comparing experiments with the material models

Section 3.2.4 described how both the extended Nadai and Bergström models predicted the material behaviour in case of a strain rate jump. In Figure 3.6 it could be seen that the extended Nadai model predicts an immediate response of the material, while the Bergström model predicts a slow approach of the constant strain rate curve.

As illustrated in Figure 5.6, the material behaviour is somewhere in the middle: there is an immediate response as predicted by the extended Nadai model, followed by a slower response as predicted by the Bergström model. For higher temperatures (250 °C) there is a larger immediate response, which means that the extended Nadai model predicts this behaviour better. This outcome is surprising as the extended Nadai model is a phenomenological model and is based on responses of the model to a constant strain rate and temperature. The Bergström model, however, is physically based, and it was expected that it would therefore predict the material behaviour during a strain rate jump better. However, this is not the case, so it is suggested that further research is conducted during which this material model is investigated further to see if by including more information in the model, e.g. the observed temperature dependence of the response to a jump in the strain rate, it can be improved.

Chapter 6

Conclusions and recommendations

In this chapter the conclusions from the current research and recommendations for future research are presented.

6.1 Conclusions

To model the material behaviour of aluminium-magnesium alloys at elevated temperatures a phenomenological model (the extended Nadai model) and a physically based model (the Bergström model) were presented and used in this thesis. The parameters of these models were determined by fitting the models to stress-strain curves obtained from constant strain rate tests performed at TNO Eindhoven for various temperatures and strain rates. For constant strain rate both models predicted the stress-strain curves reasonably accurate. The Bergström model describes the material behaviour slightly better than the extended Nadai model.

When using the Bergström model in a finite element simulation, it was seen that the model is able to describe the material behaviour of aluminium in uniaxial deformation at elevated temperatures and constant strain rates successfully. The stress-strain curves were predicted accurately up to the ultimate tensile strength. After necking the numerical simulations have approximately the same softening slope as the experimental results, although in the numerical analysis localisation starts earlier.

When a strain rate jump is applied, the two material models predict completely different responses. The extended Nadai model predicts an instantaneous stress jump, whereas the Bergström model predicts a gradual change in stress until the curve that corresponds to the new strain rate is reached. Experiments that have been performed at the University of Twente showed that the actual material behaviour is somewhere in the middle: there is an immediate response as predicted by the extended Nadai model, followed by a slower response as predicted by the Bergström model. For higher temperatures (250 °C) there is a larger immediate response, which means that the extended Nadai model predicts this behaviour better.

6.2 Recommendations

Strain rates and temperatures are usually not constant during forming processes at elevated temperatures. For numerical simulations a model that describes the material behaviour in case of a strain rate jump more accurately should be developed. It is therefore recommended that the Bergström model is investigated further to see if it can be improved by including more information into the model, e.g. the observed temperature dependence of the response to a jump in the strain rate.

Since the material behaviour changes significantly between 175 °C and 250 °C it is recommended that more experiments with a strain rate jump are performed at intermediate temperatures. Next to that, it could also be useful to investigate the material behaviour at somewhat lower temperatures to see if the Bergström model is more accurate at lower temperatures. For these experiments the furnace should be covered, to decrease the temperature gradient over the specimen, which makes the test results more easy to compare with other experiments. It is also recommended that when further tests are performed a more sophisticated feedback system for the furnace is developed. As a result the heating of the specimens will be easier to regulate.

A final recommendation that can be made is to update the software used to control the tensile testing machine. When this is implemented it is possible to not only perform experiments with a single or even multiple strain rate jumps, but also to perform tensile tests with a gradual change in strain rate. It would be interesting to know how the material behaves when deformed in this way since this gives an even better approximation of the deep drawing process.

Bibliography

[1] Bergström, Y. Dislocation model for the stress-strain behaviour of polycrystalline α-Fe with special emphasis on the variation of the densities of mobile and immobile dislocations. *Mater. Sci. Eng. 5* (1969), 193–200.

[2] Bergström, Y. The plastic deformation of metals - a dislocation model and its applicability. *Reviews on Powder Metalurgy and Physical Ceramics 2* (1983), 105–115.

[3] Bolt, P. J., Lamboo, N. A. P. M., and Rozier, P. J. C. M. Feasibility of warm drawing of aluminium products. In *Sheet Metal 1999* (Erlangen, 1999), M. Geiger, H. J. J. Kals, B. Shirvani, and U. P. Singh, Eds., pp. 575–580.

[4] Bolt, P. J., Werkhoven, R. J., and Van den Boogaard, A. H. Effect of elevated temperatures on the drawability of aluminium sheet components. In *Proceedings 4th Esaform Conference* (Liege, 2001).

[5] Boyer, H. E., Ed. *Atlas of stress-strain curves.* ASM International, 1987. ISBN 0-87170-240-1.

[6] Callister, W. D. *Materials science and engineering.* John Wiley and Sons, Inc., 1985.

[7] Davis, J. R., Ed. *ASM Speciality Handbook, Aluminum and aluminum alloys.* ASM International, 1993. ISBN 0-87170-496-X.

[8] Estrin, Y. Dislocation-density–related constitutive modeling. In *Unified Constitutive Laws of Plastic Deformation*, A. S. Krausz and K. Krausz, Eds. Academic Press, San Diego, 1996, pp. 69–104.

[9] Han, P., Ed. *Tensile testing.* ASM International, 1992. ISBN 0-87170-440-4.

[10] Hertzberg, R. W. *Deformation and fracture mechanics of engineering mechanics.* John Wiley and Sons, Inc., 1989.

[11] Krabiell, A., and Dahl, W. Zum Einfluss von Temperatur und Dehngeschwindigkeit auf die Streckgrenze von Baustählen unterschiedlicher Festigkeit. *Archiv für das Eisenhüttenwesen 52* (1981), 429–436.

[12] Kuhn, H., and Medlin, D., Eds. *ASM Handbook, Volume 8: Mechanical testing and evaluation.* ASM International, 2000. ISBN 0-87170-389-0.

[13] Miller, W. S., Zhuang, L., Bottema, J., Wittebrood, A. J., de Smet, P., Haszler, A., and Vieregge, A. Recent developments in aluminium alloys for the automotive industry. *Materials Science and Engineering A 280* (2000), 37–49.

[14] Nelder, J. A., and Mead, R. A simplex method for function minimization. *Computer Journal 7* (1965), 308–313.

[15] Olivier, J. G. J., Brandes, L. J., Peters, J. A. H. W., and Coenen, P. *Greenhouse gas emissions in the Netherlands 1999-2000.* RIVM, Bilthoven, 2002.

[16] Rietman, A. D. *Numerical Analysis of Inhomogeneous Deformation in Plane Strain Compression.* PhD thesis, University of Twente, 1999.

[17] Stiomak/tht. *Materiaalkeuze in de werktuigbouwkunde.* Stam Technische Boeken, Culemborg, 1978.

[18] van den Boogaard, A. H. *Thermally enhanced forming of aluminium sheet.* PhD thesis, University of Twente, 2002.

[19] van den Boogaard, A. H., Bolt, P., and Werkhoven, R. J. Aluminum sheet forming at elevated temperatures. In *Simulation of Materials Processing: Theory, Methods and Applications* (Lisse, 2001), K.-I. Mori, Ed., A.A. Balkema, pp. 819–824.

[20] van den Boogaard, A. H., Werkhoven, R. J., and Bolt, P. Modelling of AlMg sheet forming at elevated temperatures. In *International Journal of Forming Processes* (2001), vol. 4, pp. 361–375.

[21] van Liempt, P. Workhardening and substructural geometry of metals. *J. Mater. Process. Technol. 45* (1994), 459–464.

Acknowledgements

This thesis is written to conclude my studies of Mechanical Engineering at the University of Twente and is the result of an extended research period at the section Mechanics of Forming Processes.

I would like to thank everyone who has supported me and made a contribution to this graduation project. Especially I would like to thank the following people:

- My supervisor, Ton van den Boogaard, for his support, suggestions and helpful discussions.
- Erik van der Ven and Joop Brinkman for their help with the experimental part of this project and the many interesting discussions.
- Joop Brinkman again for taking care of the design and manufacturing of the clamps and test specimens and proof-reading this report.
- Jaco van Leeuwen and Peter de Maat from TNO Eindhoven who performed the uniaxial tensile tests for a constant strain rate.
- My family and friends because of their continuous support and patience.
- Finally I would like to thank the fellow students with whom I cooperated during most of my studies in our project team and the students and members of the section Mechanics of Forming Processes for giving me a pleasant time during my studies.